Materials Today Bio 13 (2022) 100206

Contents lists available at ScienceDirect

Materials Today Bio

journal homepage: www.journals.elsevier.com/materials-today-bio

Sustained release of naringin from silk-fibroin-nanohydroxyapatite scaffold for the enhancement of bone regeneration

Zhi-hu Zhao [a], Xin-long Ma [a,*], Jian-xiong Ma [b], Jia-yu Kang [c], Yang Zhang [b], Yue Guo [b]

[a] Department of Orthopaedics, Tianjin Hospital, No. 406, Jiefangnan Road, Hexi District, Tianjin, 300000, China
[b] Tianjin Institute of Orthopedics in Traditional Chinese and Western Medicine, No. 122, Munan Road, Tianjin, 300050, China
[c] Department of Orthopedics, Jinhua Municipal Central Hospital, Jinhua, Zhejiang Province, China

ARTICLE INFO

Keywords:
Naringin
Silk
Hydroxyapatite
Bone defect
PLGA
Microsphere

ABSTRACT

Bone defects are a common challenge in the clinical setting. Bone tissue engineering (BTE) is an effective treatment for the clinical problem of large bone defects. In this study, we fabricated silk fibroin (SF)/hydroxyapatite (HAp) scaffolds inlaid with naringin poly lactic-co-glycolic acid (PLGA) microspheres, investigating the feasibility of their application in BTE. Naringin PLGA microspheres were manufactured and adhered to the SF/HAp scaffold. Bone mesenchymal stem cells (BMSCs) were inoculated onto the SF/HAp scaffold containing naringin PLGA microsphere to examine the biocompatibility of the SF/HAp scaffolds. A rabbit femoral distal bone defect model was used to evaluate the in vivo function of the SF/HAp scaffolds containing naringin-loaded PLGA microspheres. The current study demonstrated that SF/HAp scaffolds containing naringin-loaded PLGA microspheres show promise as osteo-modulatory biomaterials for bone regeneration.

1. Introduction

Large bone defects are difficult to self-repair and frequently require specific and costly management [1,2]. Moreover, autogenous or allogeneic bone grafts have certain drawbacks. Bone tissue engineering (BTE) has the potential to repair bone defects and has thus drawn considerable attention [3,4]. BTE requires three components: combining biomaterials, appropriate bioactive molecules, and cells. Although satisfactory outcomes have been achieved, upscaling BTE for clinical applications is limited for various reasons.

An ideal biomaterial for bone defect healing should be biodegradable, biocompatible, and have a favorable bone-promoting microenvironment [5]. These scaffold characteristics can promote stem cell ingrowth and differentiation. Thus, scaffolds designed for BTE must be biocompatible and have suitable material properties [6,7].

Thus, several studies have fabricated silk fibroin (SF)/hydroxyapatite (HAp) composite scaffolds for BTE via different approaches [8,9]. SF, a natural protein, has broad application prospects in the field of biomaterials [10]. HAp is the main mineral component in mammalian bones and is considered an ideal bone repair material. SF was coupled with HAp to obtain porous composite scaffold materials [11]. In our previous study, an SF/HAp biological composite scaffold mixed with naringin was designed and fabricated as a carrier for human umbilical cord-derived mesenchymal stem cells to effectively repair bone defects [12]. During the manufacturing procedure, silk was dissolved in hexafluoroisopropyl, an organic solvent. However, hexafluoroisopropyl is toxic to humans and causes other undesirable side effects. Therefore, the development of nontoxic solvents for dissolving SF and HAp is necessary for clinical applications.

Naringin is the main ingredient of the root *Rhizoma Drynariae* and has the potential to promote osteoblast differentiation of mesenchymal stem cells and precursor cells of osteoblasts [13,14]. Moreover, naringin could induce osteoclast apoptosis and thus be administered for the prevention and treatment of osteoporosis [15,16]. Therefore, naringin is widely used for the prevention and treatment of osteoporosis and related bone diseases [17–20]. Naringin was previously found to promote angiogenesis in

Abbreviations: BTE, Bone tissue engineering; SF, silk fibroin; HAp, hydroxyapatite; PLGA, poly lactic-co-glycolic acid; BMSCs, Bone mesenchymal stem cells; HUVEC, human umbilical endothelial cells; PVA, Polyvinyl alcohol; SEM, scanning electron microscopy; CCK-8, Cell count kit-8; ALP, Alkaline phosphatase activity; RNA-Seq, RNA sequencing; GO, Gene ontology; BP, biological process; CC, cellular component; MF, molecular function; KEGG, Kyoto Encyclopedia of Genes and Genomes; DAVID, database for annotation, visualization, and integrated discovery; RT-PCR, real-time quantitative polymerase chain reaction; ANOVA, one-way analysis of variance.

* Corresponding author. Department of Orthopaedics, Tianjin Hospital, No. 406, Jiefangnan Road, Hexi District, Tianjin, 300000, China.
E-mail address: gukezzh@126.com (X.-l. Ma).

https://doi.org/10.1016/j.mtbio.2022.100206
Received 29 November 2021; Received in revised form 14 January 2022; Accepted 17 January 2022
Available online 23 January 2022

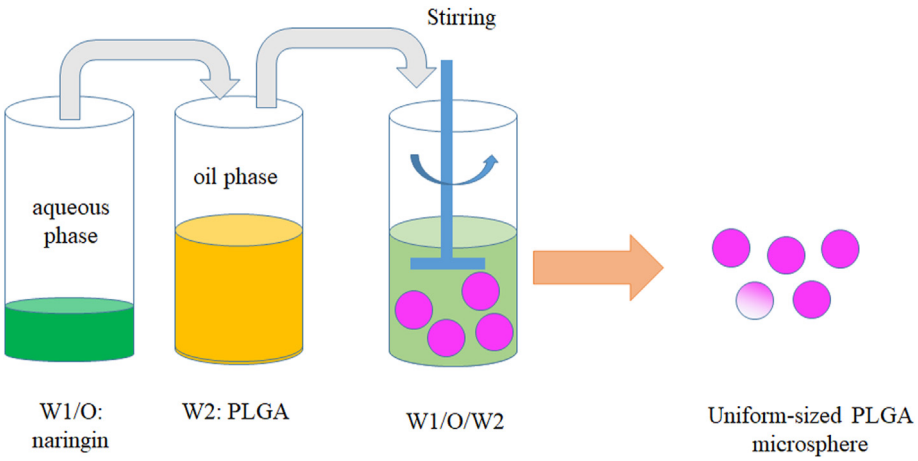

Fig. 1. Schematic illustration of the fabrication process of naringin-loaded PLGA microspheres.

diabetic foot ulcers in rats by regulating inflammatory and growth factor expression [21]. It has been reported that naringin can potentially promote vascularization and bone regeneration when used in osteoporotic bone fracture models [21,22]. Naringin can also regulate the differentiation of endothelial progenitor cells differentiation through a CXCR4-regulated PI3K/Akt signaling pathway [23]. Naringin possess the feature properties to repair large segmental bone defects, including osteostimulation (promoting new bone formation) and angiostimulation (inducing vascularization). Our previous study reported that naringin-inlaid SF/HAp scaffolds enhance osteogenic differentiation of human umbilical cord-derived mesenchymal stem cells and can be used to treat bone defects [12]. The scaffolds also enhance angiogenesis of human umbilical endothelial cells (HUVEC). These findings suggest that naringin may be an effective candidate drug for treating the most common bone diseases and defects.

However, the naringin/SF/HAp scaffold led to a burst release of over 70% naringin within 20 h. The burst release may lead to systemic toxicity [24,25]. Moreover, naringin displays low bioavailability due to its poor aqueous solubility [26,27]. Finally, the drug was rapidly cleared from the bone defect area, which prompted the development of a long-acting, controlled release system for releasing naringin.

Poly lactic-co-glycolic acid (PLGA) microspheres have been suggested to be highly suitable as sustained-release carriers of medical materials, drugs, and cytokines [28,29]. PLGA microspheres have been employed as injectable carriers to promote bone defect healing repair [30]. In the present study, we developed a novel SF/HAp scaffold capable of releasing naringin in a controlled manner. A composite of SF and HAp porous scaffolds was used to incorporate naringin-encapsulated PLGA microspheres that were prepared via the emulsion-solvent evaporation method to achieve the high encapsulation efficacy of naringin.

Bone mesenchymal stem cells (BMSCs) were used to evaluate the effect of the SF/HAp composite scaffold on the osteogenic differentiation of BMSCs and further investigate the bone defect repair characteristics in vivo with the SF/HAp composite scaffold in a rabbit femoral condyle defect model.

2. Materials

2.1. Preparation of PLGA microspheres loaded naringin

PLGA (lactide/glycolide = 50:50; molecular weight = 94,000 Da) was purchased from Jinan Daigang Biomaterial Co. (Jinan, Shandong, China). Polyvinyl alcohol (PVA) was purchased from Sigma-Aldrich (Shanghai, China). Naringin (purity ≥98%) was obtained from Sigma-Aldrich (St. Louis, MO, USA).

PLGA microspheres incorporated with naringin were prepared using the water-in-oil-in-water (w/o/w) emulsion solvent evaporation method (Fig. 1).

In brief, 500 mg PLGA (lactide:glycolide = 50:50, Mw = 94,000 Da) was dissolved in 3 mL dichloromethane (≥99.9% chemical purity, 3rd Branch of Tianjin Chemical Reagent Co., Ltd, Tianjin, China) to form a PLGA solution.

Naringin (10 mg) was dissolved in 0.1 mL methyl alcohol (100 mg/mL, ≥99.9% chemical purity, Tianda Tianjin Chemical Reagent Factory, Tianjin, China) to obtain a naringin solution. These two solutions were mixed using a homogenizer (XR-C200S; Shanghai Muxuan Co., Ltd., China) for 1 min at 10,000 rpm to form the primary emulsions.

This solution was dropped into 300 mL of 0.25% (w/v) PVA solution at room temperature and homogenized for 5 min using a homogenizer (XR-C200S; Shanghai Muxuan Co., Ltd., China) at 10,000 rpm. A 0.25% (w/v) PVA solution (Mw 9000–10,000, 80% hydrolyzed from Aldrich) was prepared by dissolving PVA in deionized water at 80 °C with stirring for 6 h.

An emulsion was formed and continuously stirred for 8 h at room temperature to evaporate the organic solvent. The microsphere suspension was centrifugated at 6000 rpm for 15 min, and the microspheres were washed three times with distilled water. Finally, microspheres were frozen to −80 °C, lyophilized at −80 °C using a lyophilizer (Alpha 1–2 LDplus, CHRIST, Germany) for 24 h.

2.2. Microsphere characterization

The surface appearance and inner structure of the microspheres were examined by scanning electron microscopy (SEM, S-4300, Hitachi. Tokyo, Japan). Nano Measure software (Nano Measure 1.2) was used to calculate the particle size of 100 randomly selected nanorod SEM images. The size distribution was obtained using Origin 7.5 software (Origen Lab Corporation, Northampton, MA, USA).

2.3. Naringin loading efficiency and encapsulation efficiency test

PLGA microspheres (500 mg) were dispersed in 1 mL of NaOH (0.04 M) solution to release naringin loaded into the PLGA microspheres. Next, the concentration of naringin in the solution was determined using a microplate fluorometer at 282 nm, according to a previous report [31]. The naringin loading efficiency and encapsulation efficiency were calculated using the following equations:

$$\text{Loading efficacy (w/w)} = \frac{\text{mass of naringin in microsphere}}{\text{mass of microsphere}} \quad (1)$$

Table 1
The relevant antibody information.

Antibody	Cat No.	Dilution	Source
collagen type I A1	ab138492	1:2000	Abcam, Cambridge, UK
OCN	ab133612	1:5000	Abcam, Cambridge, UK
RUNX2	20700-1-AP	1:500	Proteintech, Wuhan, China
GAPDH	80570-1-RR	1:5000	Proteintech, Wuhan, China

$$\text{Encapsulation efficacy } (\%,\ \text{w/w}) = \frac{\text{loading efficacy}}{\text{theoretical loading efficacy}} \times 100\% \quad (2)$$

2.4. In vitro release profiles of naringin

PLGA microspheres (500 mg) or SF/HAp scaffolds with PLGA microspheres (500 mg) were dissolved in 50 mL phosphate-buffered saline (PBS, pH = 7.4) solution and maintained at 37 °C and 75 rpm in a gas bath thermostatic oscillator (KYC–1102C). At 3, 6, 12, 24, 72, 96, 120, 144, 192, 240, 288, 360, 432, 504, 576, 648, 720, 792, and 864 h, 0.5 mL was collected for absorbance determination using a UV spectrophotometer at 282 cm^{-1} and replaced with fresh 0.5 mL PBS. The release rate was calculated using a standard curve:

$$\text{Release rate } (\%) = \frac{\textit{amount is naringin released}}{\textit{amount of naringin loaded}} \times 100\% \quad (3)$$

2.5. Scaffold fabrication

Bombyx mori silkworm silk was purchased from Simatech (Suzhou, China). The SF solution was prepared as previously described [12]. Briefly, sericin was removed by boiling the cocoons in a 0.02 M Na_2CO_3 solution for 30 min. The resulting fibers were then dissolved in 9.3 M LiBr for 4 h at 60 °C and subsequently dialyzed in a dialysis bag (Cat No. YA1078, Solarbio, Beijing, China, molecular weight cut-off = 3500 Da) against ultrapure water for 48 h, with a water change every 6 h to remove residual LiBr. Finally, the SF solution was dialyzed against polyethylene glycol (PEG, Mw 20,000, Biosharp, Shanghai, China) powder to produce an SF solution with a concentration of 15%. HAp was obtained from Solarbio (Beijing, China).

The SF/HAp scaffolds were fabricated as follows: In brief, carboxylated cellulose nanofibrils (cCNF, Naxian Technology Co., Ltd., Zhongshan, Guangzhou, China) were added to a HAp solution (300 mg/mL) in a ratio of 4:1 (v/v) to maintain the stability of HAp in water. The HAp/cCNF suspension was then added to the SF solution (10% w/v) at a ratio of 1:9 (v/v) under magnetic stirring for 1 h. Finally, PLGA microspheres containing naringin (5 mg/mL) or blank microspheres were loaded into the suspension to form MSN/SF/HAp and MSB/SF/HAp, respectively. The prepared suspension (50 μL) was transferred to a mold plate and freeze-dried at −80 °C using a lyophilizer (Alpha 1–2 LDplus, CHRIST, Germany) for 24 h. Once the scaffolds solidified, they were treated with methanol for 1 d to induce β-sheet formation. Scaffolds were cut and cored into cylinders 6 mm in diameter and 10 mm thick and were ethylene oxide sterilized in scintillation vials. The abbreviations and scaffold preparations used in this study are summarized in Table 1.

The specimens used for the measurement discs were 6 mm in diameter and 10 mm in thickness, and the compressive strengths of the scaffolds were measured using an Electro-Force 3230 System (BOSE, Minnetonka, MN, USA). Briefly, SF/HAp, MSB/SF/HAp, and MSN/SF/HAp scaffolds were loaded at a constant crosshead speed of 0.5 mm/min until failure occurred.

The porosity of the scaffolds was calculated as previously described. In brief, SF/HAp, MSB/SF/HAp, and MSN/SF/HAp were weighed as dry weight (V1). All scaffolds were then immersed in PBS to determine their weight (V2). Finally, the water on the surface of the scaffolds was removed to re-weigh the wet weight (V3). The final porosity was calculated using the following equation:

$$\text{Porosity } (\%) = \frac{V1 - V3}{V2 - V3} \times 100\% \quad (4)$$

A total of 10 visual fields were randomly selected from the SEM images, and the pore diameter of the scaffolds was calculated using Nano Measure 1.2 image processing software. The pore interconnectivity (volumetric adsorption ratio) was calculated as previously described [32].

2.6. Cell culture and identification

Human BMSCs were cultured in DMEM supplemented with 10% fetal bovine serum and 1% streptomycin-penicillin. BMSC identification was performed as previously described [33]. The antibodies used for surface markers were human CD34-APC, CD45-FITC, CD13-APC, CD44-FITC, CD73-PE, and CD90-PE (Tianjin Hao Yang Biological Manufacture Co., LTD, Tianjin, China).

To identify the trilineage differentiation potential of BMSCs, BMSCs were induced to undergo osteogenic, chondrogenic, and adipogenic differentiation using osteogenic, adipogenic, and chondrogenic media (Fuyuan Bio Co., LTD, Shanghai, China), respectively.

For osteogenic and adipogenic differentiation, BMSCs at passage 3 seeded at a density of 2×10^4 cell/cm^2 into 6-well culture plates. When cell confluence reached 70%–80%, the medium was completely replaced and thereafter replaced with osteogenic or adipogenic medium every three days. After 21 days, osteogenic capacity was detected by staining with 0.2% Alizarin red S (Solarbio, China). After 10 days, adipogenic differentiation was detected by staining with Oil Red O (Solarbio).

To determine the chondrogenic potential of the BMSCs, a pellet culture system was used for chondrogenic induction. Briefly, 1×10^6 BMSCs were suspended in a 15-mL centrifuge tube at 800×*g* for 5 min, and the cell pellets were then cultured in chondrogenic induction medium for 4 weeks. To assess chondrogenic differentiation, the pellet was stained with Alcian blue solution for 30 min.

2.7. Cell count kit-8 (CCK-8)

The CCK-8 assay was used to assess cell metabolic activity following standard protocols. BMSCs (3×10^3) in 200 μL of the medium were transplanted into 96-well plates. After culturing in the SF/HAp, MSB/SF/HAp, and MSN/SF/HAp scaffolds for 1, 3, 7, 14, and 21 d, CCK-8 solution (10 μL, Solarbio, Beijing, China) was added to each well containing a 100 μL mixture of culture medium. After 2 h of incubation, absorbance was measured at 282 nm using a microplate reader (BioTek microplate reader).

2.8. Annexin V/PI staining by flow cytometry

The apoptosis of BMSCs was evaluated using an Annexin V-PI apoptosis detection kit (Invitrogen; Thermo Fisher Scientific, Inc.) according to the manufacturer's protocol.

BMSCs from the control, SF/HAp, MSB/SF/HAp, and MSN/SF/HAp scaffolds were harvested and washed twice with cold PBS three times. BMSCs in different treatment groups were resuspended in 1X binding buffer at a concentration of 1×10^6 cells/mL, and 5 μL of FITC Annexin V and 5 μL PI were added to 100 μL of the cell suspension. The mixture was then incubated for 15 min in the dark. The preparations were analyzed using flow cytometry (BD FACSAria III, San Jose, CA, USA). The apoptosis rate was calculated as:

$$\textit{Apoptosis rate} = (\textit{percentage of } Q3 \textit{ cells} + \textit{percentage of } Q2 \textit{ cells}) \times 100 \quad (5)$$

2.9. Alkaline phosphatase activity

After seven days of culture, BMSCs were fixed in 4% paraformaldehyde for 10 min, and ALP staining solution (Beyotime, Shanghai, China) was added for 20 min. After removing the ALP solution, ALP staining was visualized using a Nikon microscope (Nikon, Minato, Japan).

BMSCs were cultured in normal and osteoinductive media in the presence of SF/HAp, MSB/SF/HAp, or MSN/SF/HAp scaffolds, as described above. After seven days of culture, BMSCs were lysed using 100 μL RIPA lysis buffer. ALP activity was quantified using an ALP assay kit (Beyotime Biotechnology, China) according to the manufacturer's instructions.

2.10. Calcium content

The differentiation of BMSCs into osteoblasts on the MSN/SF/HAp scaffold was analyzed by histological staining. Briefly, passage 3 BMSCs (1×10^7 cells/mL, 100 μL) were seeded onto the SF/HAp, MSB/SF/HAp, and MSN/SF/HAp scaffolds. After incubation for 8 h, 2 mL culture medium was added to each well. The culture medium was replaced every two days, the scaffolds were obtained, and the tissue sections were used for von Kossa staining after 21 days. Quantitative analysis of von Kossa-positive area (%) was performed as previously described [34].

ARS staining was used to evaluate the deposition levels of calcium phosphate (Solaribio, Beijing, China). After 21 days of culture, the medium was discarded, and the cells were washed with PBS three times. BMSCs were then fixed with 4% paraformaldehyde (Solarbio, Beijing, China) for 10 min and stained with 0.1% ARS solution (pH 4.2) for 15 min. The reaction was terminated by treatment with PBS. The cells were visualized under a microscope. The ARS stain was then eluted and quantified using acetic acid extraction as previously described [35].

2.11. RNA sequencing (RNA-Seq) and bioinformatics analysis of transcriptomes

RNA sequencing was performed to further explore the mechanism of the SF/HAp scaffold inlaid with naringin PLGA microspheres. Samples from MSB/SF/HAp and MSN/SF/HAp on day 7 were prepared for RNA-seq. A sequencing library was constructed using the NEBNext® Ultra™ II Directional RNA Library Prep Kit (New England Biolabs, Inc., Massachusetts, USA) following the manufacturer's instructions. The library was quality controlled and quantified using the BioAnalyzer 2100 system (Agilent Technologies, USA), and 150-bp paired-end sequencing was performed using the Illumina HiSeq instrument. Use HISAT2 software (v2.0.4) was used to compare high-quality reads to the human reference genome (UCSC HG19). Gene ontology (GO) enrichment analysis included biological process (BP), cellular component (CC), and molecular function (MF). GO and Kyoto Encyclopedia of Genes and Genomes (KEGG) pathways were constructed using the database for annotation, visualization, and integrated discovery (DAVID, http://david.abcc.ncifcrf.gov/).

2.12. RNA isolation and real-time quantitative polymerase chain reaction (RT-qPCR)

RNA extraction was performed using TRIzol reagent (Invitrogen) according to the manufacturer's instructions. Next, 5 μg of RNA template was used to synthesize complementary DNA by reverse transcription to cDNA templates using the ReverTra Ace qPCR RT Kit (Toyobo Co. Ltd., Osaka, Japan). RT-qPCR was conducted with SYBR® Green Real-Time PCR Master Mix (Toyobo Co. Ltd., Osaka, Japan) on a LightCycler& Reg 480II real-time PCR instrument (Roche, Switzerland). RT-qPCR results were computed using the comparative threshold cycle method, with Glyceraldehyde-3-Phosphate Dehydrogenase (GAPDH) as an internal control. The primer sequences were as follows: GAPDH, 5′-GAAGGTGAAGGTCGGAGTC-3' (up) and 5′-GAGATGGTGATGGGATTTC-3' (down); OSX, 5′-CCTCCTCAGCTCACCTTCTC-3' (up) and 5′-GTTGGGAGCCCAAATAGAAA-3' (down); RUNX2, 5′-TCTTAGAACAAATTCTGCCCTTT-3' (up) and 5′-TGCTTTGGTCTTGAAATCACA-3' (down); COL1A, 5′-GCTGATGATGCCAATGTGGTT-3' (up), and 5′-CCAGTCAGAGTGGCACATCTTG-3' (down).

Table 2
Abbreviations and the preparation of the scaffold.

Name of sample	Description of sample
Control	Only administrated with osteogenic medium
SF/HAp	Original scaffold of SF/HAp without any biomolecules
MSB/SF/HAp	Scaffold with blank encapsulated into PLGA microsphere
MSN/SF/HAp	Scaffold with naringin encapsulated into PLGA microsphere

2.13. Western blot assay

Briefly, ice-cold RIPA lysis buffer (Beyotime, Shanghai, China) was used to lyse BMSCs, followed by sodium dodecyl sulfate polyacrylamide gel electrophoresis. Then, the wet electrophoretic transfer method was performed to shift the isolated protein onto nitrocellulose membranes (Bio-Rad), which were then blocked with a 5% skim milk solution. After incubation with a specific primary antibody, the membranes were probed with anti-rabbit IgG (#7074 S; 1:2000 dilution) for 1.5 h at room temperature. Finally, antibody binding was analyzed by an enhanced chemiluminescence detection kit (Pierce Biotechnology, Rockford, IL, USA). Relevant antibody information is shown in Table 2.

2.14. Immunofluorescence

According to different treatments, BMSCs were divided into control, SF/HAp, MSB/SF/HAp, and MSN/SF/HAp groups. BMSCs cultured on coverslips were fixed with 4% paraformaldehyde and washed thrice with PBS. To permeabilize the cell membranes, the cells were incubated in Triton (0.5% in phosphate-buffered saline [PBS]) at room temperature for 25 min. The samples were blocked in PBS containing 1% bovine serum albumin (BSA) for 30 min. Samples were then incubated with mouse monoclonal IgG-anti runt-related transcription factor 2 (Runx2, dilution 1:200, Abcam, Cambridge, MA, USA), osteocalcin (Ocn, dilution 1:200, Abcam), Notch1 (1:200, Abcam, USA), and Hes1 (1:200, Abcam, USA) overnight at 4 °C overnight. After washing, the cells were incubated with FITC- or TRITC-conjugated secondary antibodies at a dilution of 1:200 at 37 °C for 1 h and washed three times with PBS. Finally, the samples were incubated with DAPI (10 μg/mL, Cat No. C0065; Solarbio, Beijing, China) for 3 min for nuclear staining, and the signal was detected using an Olympus Fluoview FV1000 confocal laser scanning microscope (Olympus Life Science Europa, Tokyo, Japan).

2.15. Surgical procedure

The study protocol was approved by the ethical committee of Tianjin Hospital (IRB No. 2021YLS197) and complied with the Animal Research: Reporting of In Vivo Experiments (ARRIVE) animal research guidelines (https://arriveguidelines.org/arrive-guidelines) [36]. New Zealand white male rabbits aged 2 months and weighing 2.3–2.5 kg were purchased from the Experimental Animal Centre of Tianjin Hospital. Critically sized defects of the distal femoral epiphysis (6 mm in diameter, 10 mm in depth) were induced as previously described [12]. The rabbits were anesthetized via intramuscular injection of xylazine hydrochloride (0.2 mL/kg, Shengda, Jilin Province, China). After disinfection, the lateral femoral condyle was exposed using the lateral approach. A bicortical channel was gradually widened to a diameter of 6.0 mm with a slow-speed electric drill irrigated with ice saline solution to avoid thermal necrosis. The distal femur of rabbits was randomly assigned to

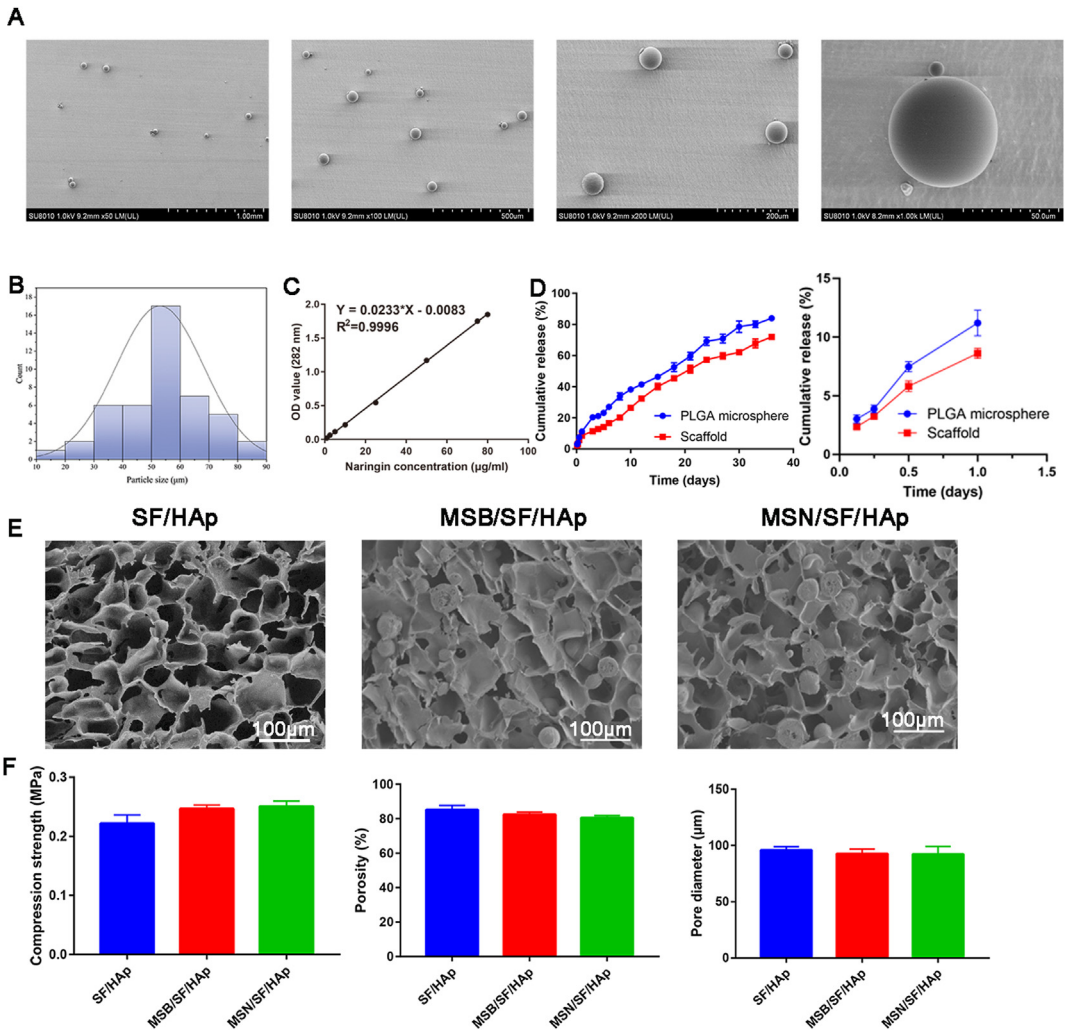

Fig. 2. A Micromorphology of microspheres loaded with naringin. B Particle size distribution of naringin-loaded PLGA microspheres. C The standard curve was drawn according to the OD values of the standard groups, and the formula was then generated based on the standard curve. D Cumulative in vitro release profile of naringin from PLGA microspheres and MSN/SF/HAp scaffolds. E Microstructures of SF/HAp, MSB/SF/HAp, and MSN/SF/HAp containing. (F) Compression strength, porosity, and pore diameter of the SF/HAp, MSB/SF/HAp, and MSN/SF/HAp scaffolds.

control (n = 3, 6 legs), SF/HAp scaffold (n = 3, 6 legs), MSB/SF/HAp scaffold (n = 3, 6 legs), and MSN/SF/HAp scaffold (n = 3, 6 legs).

After the wound was flushed with saline, it was sutured layer by layer. To avoid wound infection, each animal was administered an intramuscular injection of penicillin (100,000 U/day) per day for three days after the operation.

2.16. Micro-computed tomography

Six weeks post-implantation, the implants were harvested, fixed in 4% paraformaldehyde, decalcified with 15% EDTA, and embedded in paraffin. Micro-CT analysis (Siemens, Berlin, Germany) was performed in five samples of each group on the defect area to determine the extent of bone defect healing. 3D reconstruction and modeling techniques were automatically performed. Measurements of callus properties in the ROI included bone volume (BV, mm^3)/total volume (TV, mm^3), trabecular thickness (TB.TH), trabecular separation (TB.SP), bone surface (BS)/BV, and bone mineral density (BMD, mg/cm^3).

2.17. Histologic processing and histomorphometry

After micro-CT scanning and analysis, the harvested samples were decalcified with 15% EDTA (Beijing Solarbio Science and Technology Co., Ltd., Beijing, China, pH 7.4) and dehydrated with 70–100% ethanol (Tianjin Fuyu Fine Chemical Co. Ltd., Tianjin, China). The tissues were processed, embedded in paraffin, and cut into 5-μm sections using a routine procedure. Dehydrated sections were made transparent using xylene I and xylene II (Xian Chemical Reagents Instruments, Inc., Xian, P.R. China, 5 s each). The samples were dehydrated by 30%, 50%, 70%, 80%, and 95%, ethanol (Tianjin Fuyu Fine Chemical Co. Ltd., Tianjin, China) for 10 min and 100% for 1 h at 4 °C. Histological sections of 5 μm were performed on tissue immersed in paraffin and stained with hematoxylin-eosin, toluidine blue, and safranin O, as previously reported.

To analyze COL1A1 expression of the tissue, immunohistochemical staining was performed on paraffin sections. Briefly, endogenous peroxidase activity was quenched by treatment with 3% H_2O_2 for 10 min (Tianli Chemical Reagent Co. Ltd., Tianjin, China). For the immunohistological analyses, bone sections were subjected to optimal antigen retrieval using citric acid buffer (10 mM citric acid) for 10 min at 98 °C. H_2O_2 (30%) was diluted with PBS to a final concentration of 3% H_2O_2.

Non-specific protein binding was blocked by adding 5% BSA and then incubated with primary antibodies against COL1A1 (mouse anti-rabbit, 1:2500; Proteintech, Wuhan, China) at 4 °C overnight. Signals were developed using a 3,3-diaminobenzidine tetrahydrochloride kit (Boster, Wuhan, China). Images were captured using a microscope (Nikon).

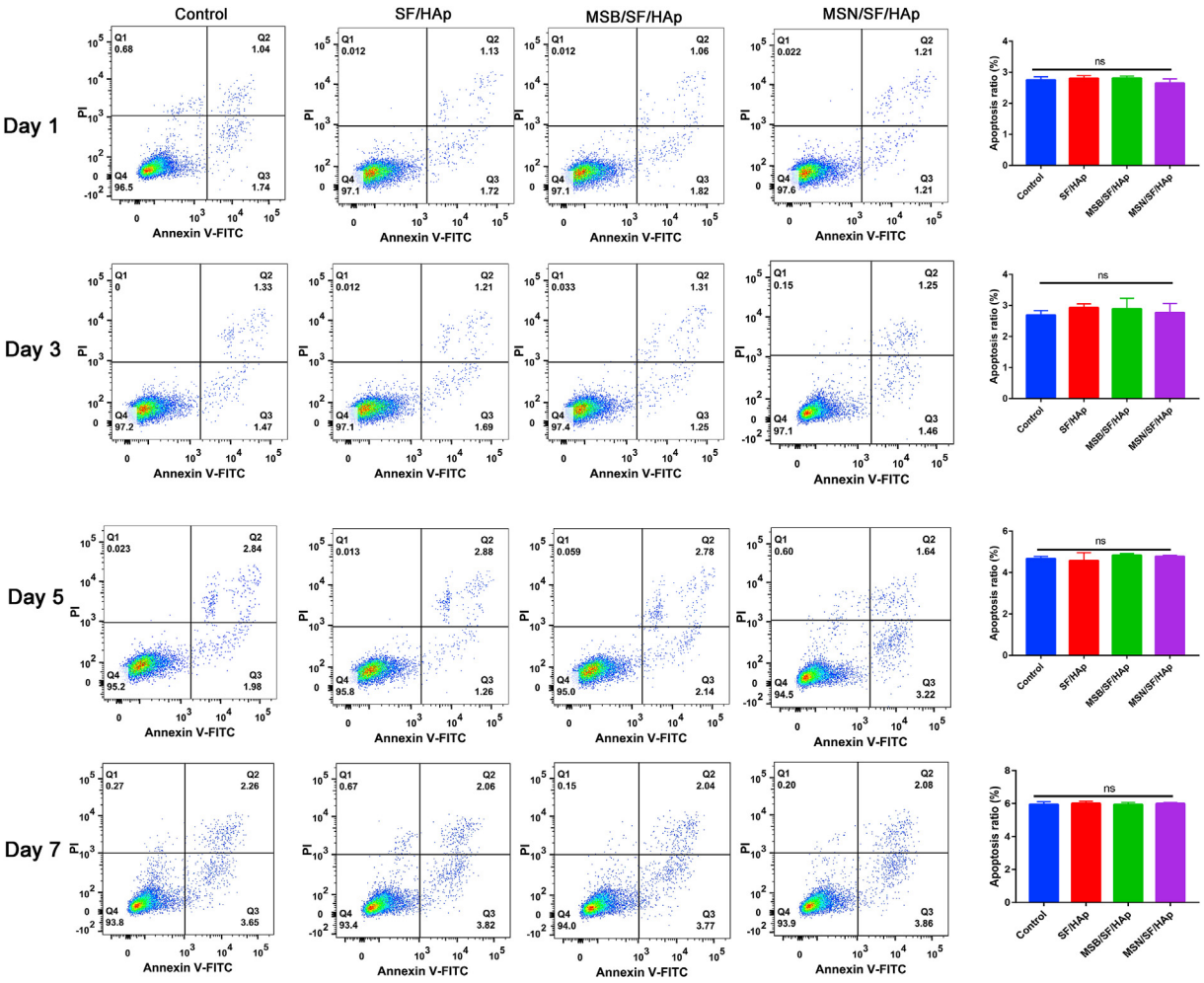

Fig. 3. Apoptosis ratio of BMSCs that seeded onto the SF/HAp, MSB/SF/HAp, and MSN/SF/HAp was quantified with an Annexin V-FITC cell apoptosis kit for 1, 3, 5 and 7 days.

2.18. Statistical analysis

Statistical analysis was performed using the SPSS software (version 22.0; IBM SPSS, Armonk, NY, USA). Statistical significance for multiple group comparisons was determined by one-way analysis of variance (ANOVA) followed by Tukey's post hoc test to compare treatments. The significance level was set at $P < 0.05$.

3. Results

3.1. Microsphere characterization and release test

The morphology of the PLGA microspheres was observed by SEM (Fig. 2A). The microspheres showed a regular spherical shape, and the diameter of the microsphere was 53.0 ± 15.1 μm (Fig. 2B). Naringin concentration curves are shown in Fig. 2C. The naringin concentration showed a linear correlation with the absorbance values ($Y = 0.0233 \times X - 0.0083$, $R^2 = 0.9996$). The loading efficiency of naringin in the PLGA microspheres was 0.01634 ± 0.0008 (mg naringin/mg PLGA). The encapsulation efficiency was 78.5 ± 3.6%. The in vitro release profile of naringin from the microspheres and MSN/SF/HAp scaffolds is shown in Fig. 2 D. During the first 24 h of incubation, approximately 11.2% of naringin was released from the PLGA microspheres, and 8.62% of naringin was released from the scaffold. The release of PLGA microspheres slowed, and approximately 83.9% and 71.9% were released from the microspheres and scaffolds, respectively, after 36 days of incubation.

The microstructure of the scaffold was further observed using SEM, as shown in Fig. 2 E, SF/HAp scaffolds were porous, and the pores were connected. The microspheres were evenly dispersed in the MSB/SF/HAp and MSN/SF/HAp scaffolds. The inclusion of microspheres did not affect the formation of the porous structures. There was no statistically significant difference between the compressive strengths of the SF/HAp, MSB/SF/HAp, and MSN/SF/HAp scaffolds (Fig. 2 F, $P > 0.05$).

The mean diameters of the SF/HAp, MSB/SF/Hap, and MSN/SF/HAp were 100.5 ± 4.5 μm, 98.7 ± 4.2 μm, and 99.4 ± 3.6 μm, respectively. As illustrated in Fig. 2 F, there is no statistically significant difference in the diameter of the three groups of SF/HAp, MSB/SF/HAp, and MSN/SF/HAp scaffolds ($P > 0.05$). The porosities of the as-fabricated scaffolds were approximately 85.2 ± 2.32%, 82.4 ± 1.32%, and 80.6 ± 1.21% for SF/HAp, MSB/SF/HAp, and MSN/SF/HAp, respectively (Fig. 2 F). The pore interconnectivities of SF/HAp, MSB/SF/HAp, and MSN/SF/HAp were 96.2 ± 0.59%, 95.0 ± 1.47%, and 94.4 ± 1.23%, respectively, indicating that the pores were all very well interconnected.

3.2. Identification of BMSCs

To further characterize human BMSCs, the cell surface markers of third-passage cells were examined by flow cytometry. BMSCs showed positive expression of MSC surface markers CD13 (98.5%), CD44 (97.7%), CD73 (95.5%), and CD90 (96.6%), and negative expression of CD34 (2.21%) and CD45 (1.98%) according to the criteria of the International Society for Cellular Therapy (Supplementary Figure. 1 A).

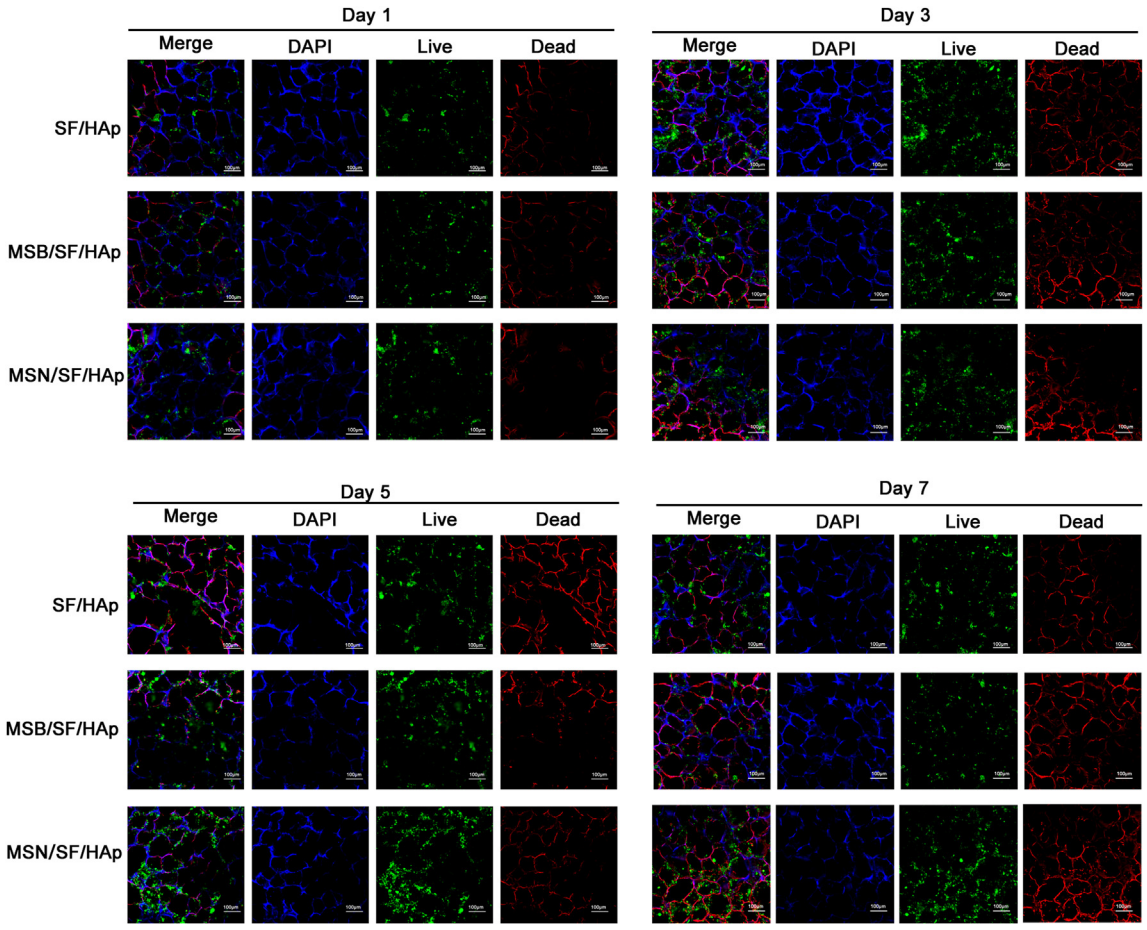

Fig. 4. After 1, 3, 5, and 7 days incubation, viable cells were monitored by Live/Dead viability and detected by fluorescence microscopy. The live cells were stained green, and the dead cells were stained red.

Analysis of the multilineage differentiation capacity of human BMSCs revealed Alizarin red staining of osteoid matrix-like structures in osteogenic medium, lipid droplet formation around the cells in adipogenic media, and Alcian blue staining of proteoglycans in chondrogenic media (Supplementary Figure. 1 B). These results indicate that the cells extracted from the human bone marrow were mainly hBMSCs.

3.3. Proliferation and viability of the hBMSCs cultured on MSN/SF/HAp scaffolds

The cell proliferation effects of the control, SF/HAp, MSB/SF/HAp, and MSN/SF/HAp scaffolds were evaluated using a CCK-8 assay kit (Supplementary Figure. 2). As shown in Supplementary Figure. 2, on days 1, 3, 7, and 21, there was no significant difference in the cell proliferation performance between the various scaffolds because cell proliferation required time. At 14 days, cell proliferation was higher in the MSN/SF/HAp group than in the SF/HAp and MSB/SF/HAp groups ($P < 0.05$).

Flow cytometry was used to investigate the apoptosis rate after the different treatments. BMSCs were cultured on each scaffold for 1, 3, 5 and 7 days, and there was no significant difference in the cell apoptosis rate between the various scaffolds at 1, 3, 5 and 7 days (Fig. 3, $P > 0.05$).

After 1, 3, 5, and 7 days of cell culture, live/dead staining results showed that the cells on the scaffold all showed green fluorescence (live cells), but only some red fluorescence (dead cells) was observed after seven days of cell culture. The number of live cells also increased with incubation time from 1 to 7 days for all scaffolds. It can be seen that the cells are evenly distributed on the wall of the scaffold hole, indicating suitable growth (Fig. 4, $P > 0.05$).

As shown in Fig. 5, the BMSCs in each sample showed a multipolar spindle-like morphology and a well-organized cytoskeleton. These results demonstrated that the treatment of cells with SF/HAp, MSB/SF/HAp, or MSN/SF/HAp scaffolds had no cytotoxicity on BMSCs, indicating that these scaffolds have good biocompatibility and biological reliability, making them suitable for tissue engineering repair. These results revealed that the SF/HAp scaffolds inlaid with naringin PLGA microspheres in this study had suitable biocompatibility and could enhance cell viability.

3.4. Osteogenic differentiation of BMSCs in the MSN/SF/HAp scaffolds in vitro

An ideal bone repair material should have good biocompatibility, mechanical strength, and osteogenic induction ability. Osteogenic differentiation of BMSCs within the MSN/SF/HAp scaffolds was examined using ALP activity, ALP staining, and Alizarin red S staining.

After seven days of culture in osteogenic medium, the SF/HAp and MSB/SF/HAp groups for both BMSCs showed enhanced ALP staining compared to that of the same cell types in the normal medium group (Fig. 6). Moreover, MSN/SF/HAp significantly enhanced osteogenesis, as indicated by the ALP staining and quantification (Supplementary Figure. 3).

The calcium salt deposition of BMSCs after incubation for three weeks was confirmed by Alizarin red staining in the control, SF/HAp, MSB/SF/

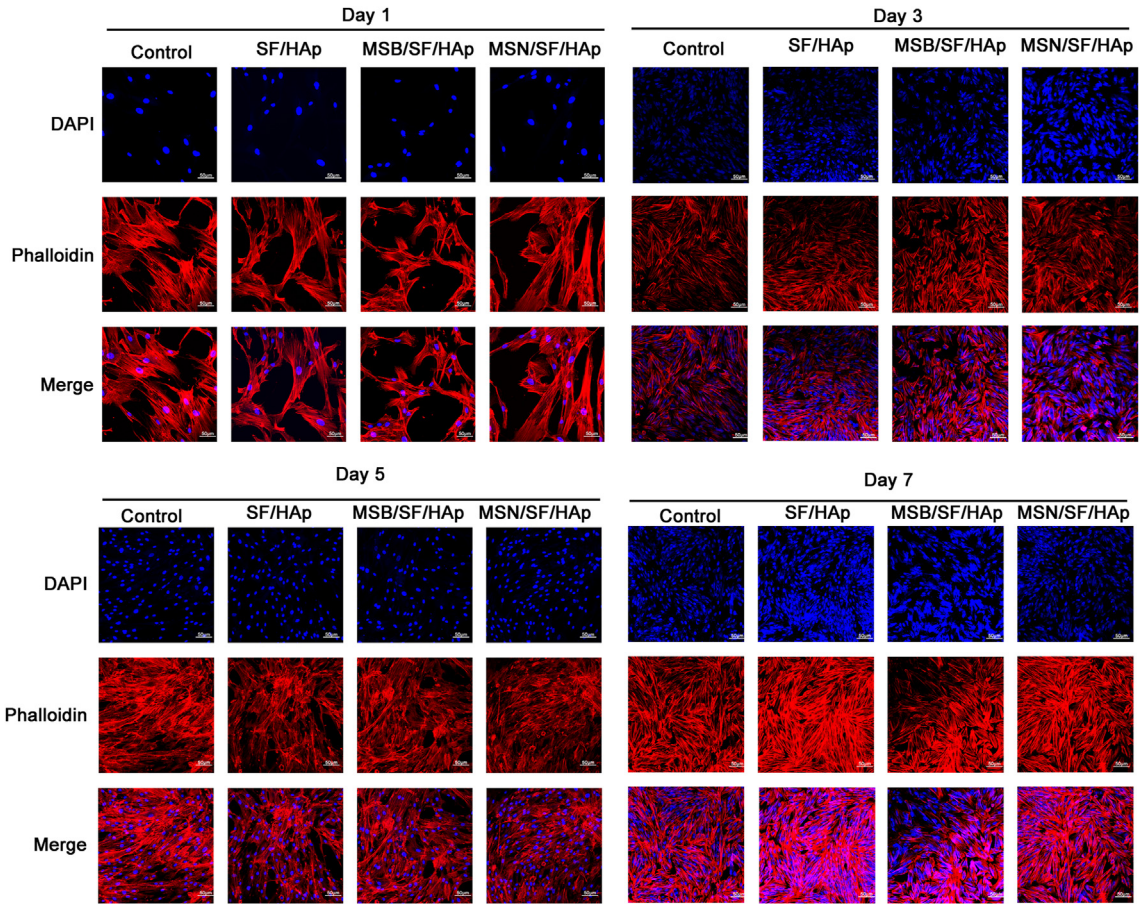

Fig. 5. BMSCs were seeded on different scaffolds for 1, 3, 5, and 7 days, stained with phalloidin (red) and DAPI (blue), and analyzed by confocal laser scanning microscopy.

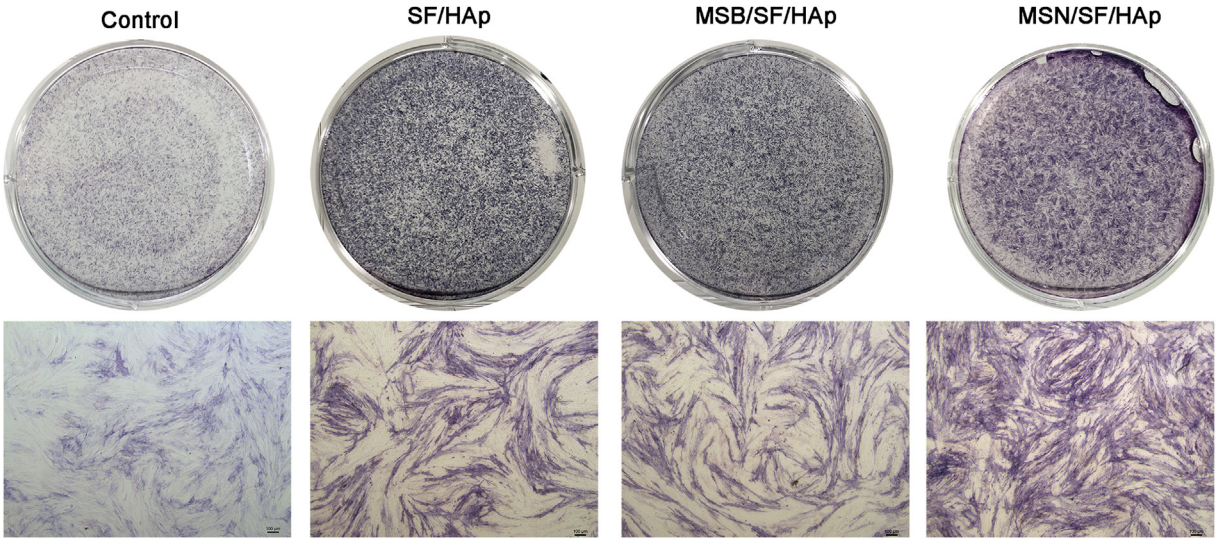

Fig. 6. ALP staining and quantification of ALP specific activities for BMSCs after 7 days of culture on control, SF/HAp, MSB/SF/HAp, and MSN/SF/HAp scaffolds (n = 3).

HAp, and MSN/SF/HAp groups (Fig. 7 and Supplementary Figure. 4). Calcium deposition was observed at three weeks in all groups; however, the amount of deposited calcium was much higher in the MSN/SF/HAp group than in the MSB/SF/HAp, SF/HAp, and control groups (all $P < 0.05$).

To evaluate the effect of MSN/SF/HAp on the osteogenic differentiation of BMSCs in vitro, the scaffold was stained with von Kossa staining 21 days after osteogenic induction. Results showed that the von Kossa-positive area was comparable, and the production by the MSN/SF/HAp group was significantly higher than that of the SF/HAp and MSB/SF/HAp groups (Supplementary Figure. 5).

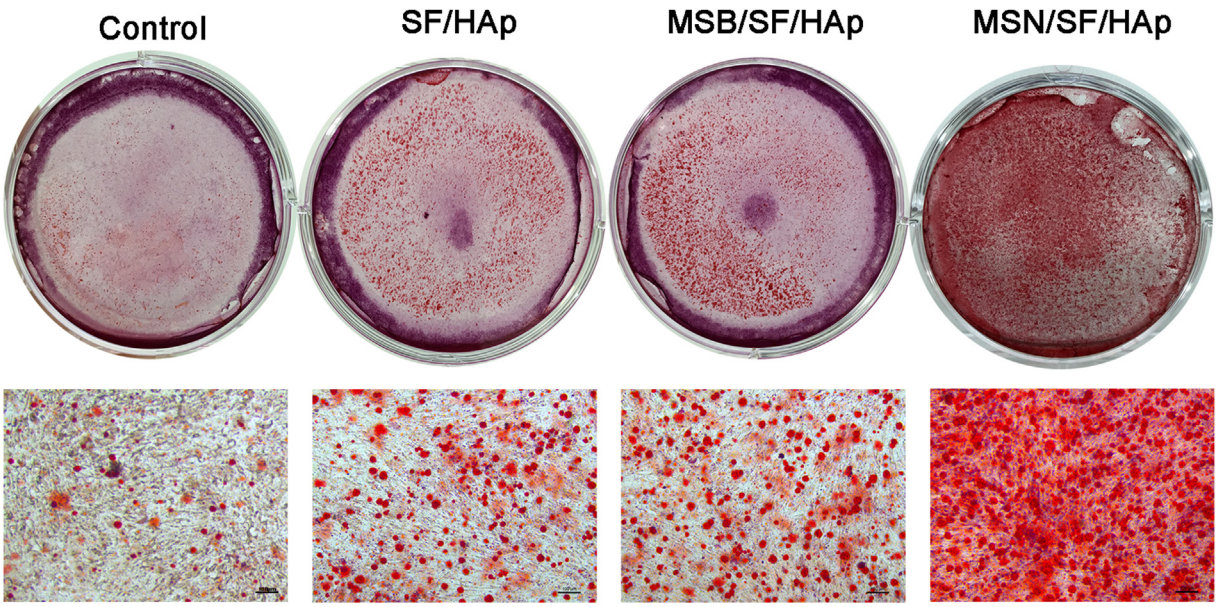

Fig. 7. Alizarin Red S staining of BMSCs after 21 days of culture on control, SF/HAp, MSB/SF/HAp, and MSN/SF/HAp scaffolds (n = 3).

To reveal the effect of MSN/SF/HAp scaffolds on the osteogenic differentiation of BMSCs in vitro, we seeded cells on control, SF/HAp, MSB/SF/HAp, and MSN/SF/HAp scaffolds. To explore the influence of MSN/SF/HAp on the differentiation of BMSCs, cells were cultured in osteogenic medium for 14 days in the presence or absence of MSN/SF/HAp, and osteogenic marker proteins in BMSCs were analyzed by RT-PCR and western blotting (Supplementary Figure. 6 A and B).

The results showed that both the SF/HAp and MSB/SF/HAp groups performed better than the control group ($P < 0.01$). The MSN/SF/HAp scaffolds promoted the expression of osteogenic markers (Runx2, BMP2, OCN) more than the SF/HAp, MSB/SF/HAp, and control. These results suggest that naringin microspheres inlaid in SF/HAp scaffolds can promote osteogenic differentiation of BMSCs. The Western blot results for osteogenic markers were consistent with the RT-PCR results.

3.5. MSN/SF/HAp scaffold activated the notch signaling pathway

We performed differential gene expression analysis of RNA sequencing data between control and MSN/SF/HAp scaffold-treated BMSCs. We identified 710 differentially expressed RNAs: 323 genes were downregulated, and 387 were upregulated (Fig. 8 A and B). Three subontologies, BP, MF, and CC, were examined using GO analysis (Fig. 8C). BP mainly includes the Notch signaling pathway, regulation of the Notch signaling pathway, regulation of cell differentiation, positive regulation of cellular processes, and regulation of cell development. CC mainly includes the transcription complex, nucleoplasm, protein-containing complex, intracellular organelle lumen, and the nucleus. MF mainly includes β-catenin binding, protein domain-specific binding, transcription factor binding, enzyme binding, and protein binding.

The top five overrepresented GO terms for the osteogenic differentiation of BMSCs induced by MSN/SF/HAp included the nucleoplasm, nucleus, enzyme binding, transcription factor, and Notch signaling pathway (Fig. 8 D).

The top ten enriched KEGG pathways included the Notch signaling pathway, pathways in cancer, endocrine resistance, PI3K/Akt signaling pathway, Wnt signaling pathway, HIF-1 signaling pathway, cell cycle, TGF-β signaling pathway, renal cell carcinoma, and breast cancer (Fig. 8 E).

To detect the protein expression of genes in the Notch signaling pathway in BMSCs, BMSCs were cultured in control, SF/HAp, MSB/SF/HAp, and MSN/SF/HAp for seven days, and the proteins were detected by Western blot analysis.

Real-time PCR was used to detect the expression of Notch signaling pathway components, including Notch1, Jagged1, and NICD (Supplementary Figure. 7 A and B).

Results revealed that the Notch1, Jagged1, and NICD expression levels in the MSN/SF/HAp group were higher than those in the control group ($P < 0.05$) and MSB/SF/HAp and SF/HAp groups ($P < 0.05$).

Compared with the control group, Notch1, Jagged1, and NICD expression levels were significantly increased in the SF/HAp, MSB/SF/HAp, and MSN/SF/HAp groups ($P < 0.05$). The expression of proteins related to the Notch signaling pathway was higher in the MSN/SF/HAp group than in the SF/HAp and MSB/SF/HAp groups (Supplementary Figure. 7C).

The expression of Notch1, Hes1, RUNX2, and OCN in BMSCs seeded on different scaffolds after 14 days was further examined by immunofluorescence. Notch1 and Hes1 staining is shown as a cytoplasmic pattern (Supplementary Figure. 8). In addition, MSN/SF/HAp showed the highest increase in RUNX2 and OCN expression compared to the other groups (Supplementary Figure. 8).

3.6. MSN/SF/HAp scaffolds regenerate bone in vivo

Six weeks later, three-dimensional reconstruction of the trabecular bone structure in the distal femur by micro-CT is shown in Fig. 9. As shown in Fig. 9, in the control group, only some fibrous tissues and a small amount of new bone formation were observed at the defect margins.

More new bone formation was observed in the SF/HAp and MSB/SF/HAp groups than in the control group. Compared with SF/HAp or MSB/SF/HAp, MSN/SF/HAp showed a superior therapeutic effect in bone defect repair.

BMD significantly increased in the MSN/SF/HAp group, followed by the MSB/SF/HAp, SF/HAp, and control groups (Fig. 9). The BMD in the control group was the lowest bone mineral density.

HE staining revealed that bone defects in the MSN/SF/HAp group showed noticeable signs of bone repair. Accumulation of collagenous fiber tissues was observed in the defect sites in the MSN/SF/HAp group compared to the control and MSB/SF/HAp groups (Fig. 10).

A small amount of new bone tissue was observed in the SF/HAp and

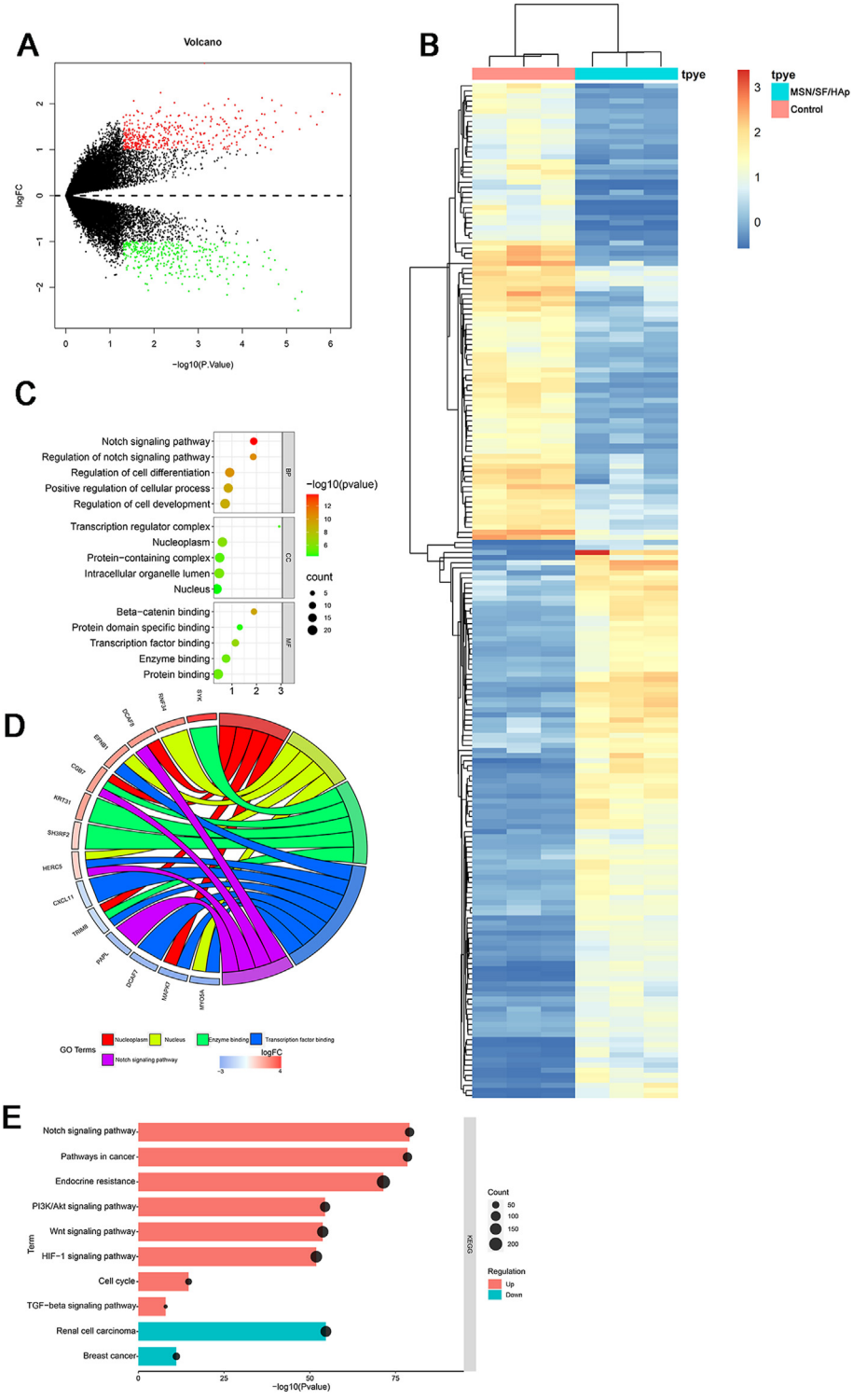

Fig. 8. A Volcano plot showing the differential expression of mRNAs in BMSCs seeded on MSN/SF/HAp scaffold. In the plot, green dots represent downregulated differentially expressed genes, red dots represent upregulated differentially expressed genes, and black dots represent non-differentially expressed genes. B Heatmap of differentially expressed mRNAs in BMSCs seeded on MSN/SF/HAp scaffolds. Red represents upregulated genes, and blue represents downregulated genes. C GO of the differentially expressed mRNAs between control and MSN/SF/HAp-treated BMSCs. D GO chord plot of top five ranked overrepresented GO terms. E KEGG pathway enrichment of differentially expressed genes.

MSB/SF/HAp groups. Moreover, the MSN/SF/HAp group showed the greatest amount of bone formation compared to the other groups.

Toluidine blue (Fig. 11) and safranin O (Fig. 12) staining further identified that the MSN/SF/HAp group was associated with more new bone formation than the other groups.

Bone matrix formation was confirmed using immunohistochemical staining for COL1A. We performed immunohistochemistry to identify COL1A expression among all groups. The results suggest many more COL1A-positive cells in the MSN/SF/HAp scaffolds than in the other groups (Fig. 13). The results indicated that the MSN/SF/HAp scaffolds significantly promoted repair of the bone defect in the rabbit distal femur bone defect and exhibited high bone regeneration efficiency.

4. Discussion

Researchers have made significant efforts to produce bone graft substitutes using tissue engineering techniques in recent years [37–40]. Unfortunately, bone repair scaffolds still have many problems, such as a low speed of bone repair and angiogenetic ability [41]. Bone is a calcified tissue composed of 35% organic matter and 65% inorganic matter [42].

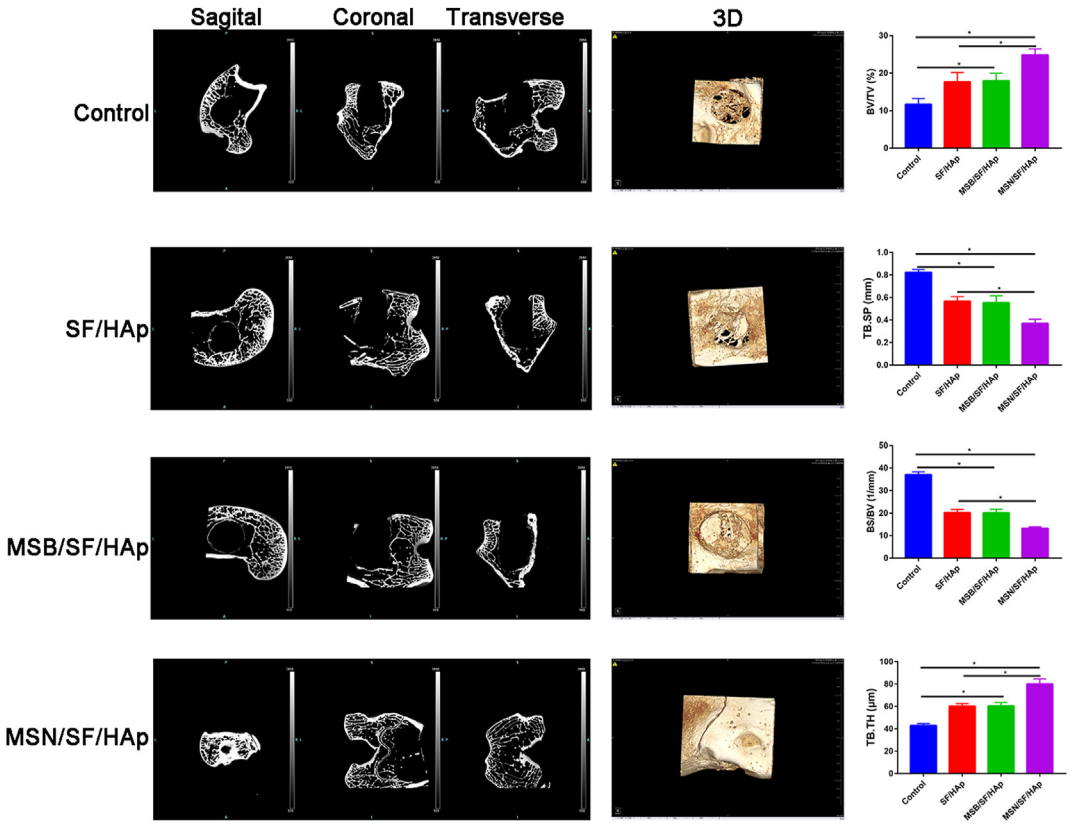

Fig. 9. Micro-CT image and quantitative analyses of BV/TV, TB. SP, BS/BV, and TB. TH were used to assess new bone formation of different scaffolds within the bone defect regions 6 weeks following scaffold implantation in the distal femoral defect rabbit model.

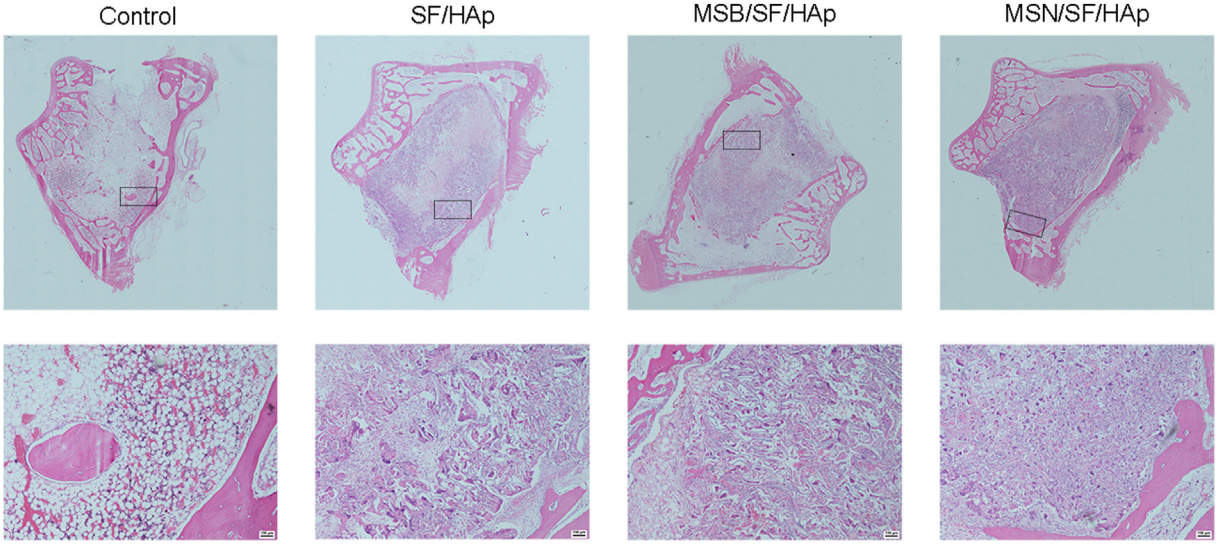

Fig. 10. HE staining of defect area after implantation with different scaffolds for 6 weeks.

The main component of inorganic substances is a type I collagen, and the main component of inorganic substances is weakly crystalline HAp [43]. SF offers biocompatibility, controllable degradation rates, and excellent mechanical properties [44–46]. HAp is extensively used as a biomaterial due to its excellent biocompatibility, bioactivity, and osteoconductivity [47,48].

In our previous study, we prepared an SF/HAp scaffold by salt leaching and inlaid it with naringin for bone formation [12]. However, three concerns remain in this study. First, a high initial burst release of naringin from the scaffold could lead to the release of the drug at toxic doses and loss of a significant amount of drug not be available for later release. Moreover, hexafluoroisopropanol was used as a solvent to produce SF solutions, which may have some potential toxic effects [49]. Third, when the mass of HAp in the SF solution increased, the stability of the suspension decreased.

For this purpose, naringin-loaded PLGA microspheres were first produced by a w/o/w solvent evaporation method. The obtained microspheres were used in an in vitro naringin release experiment and

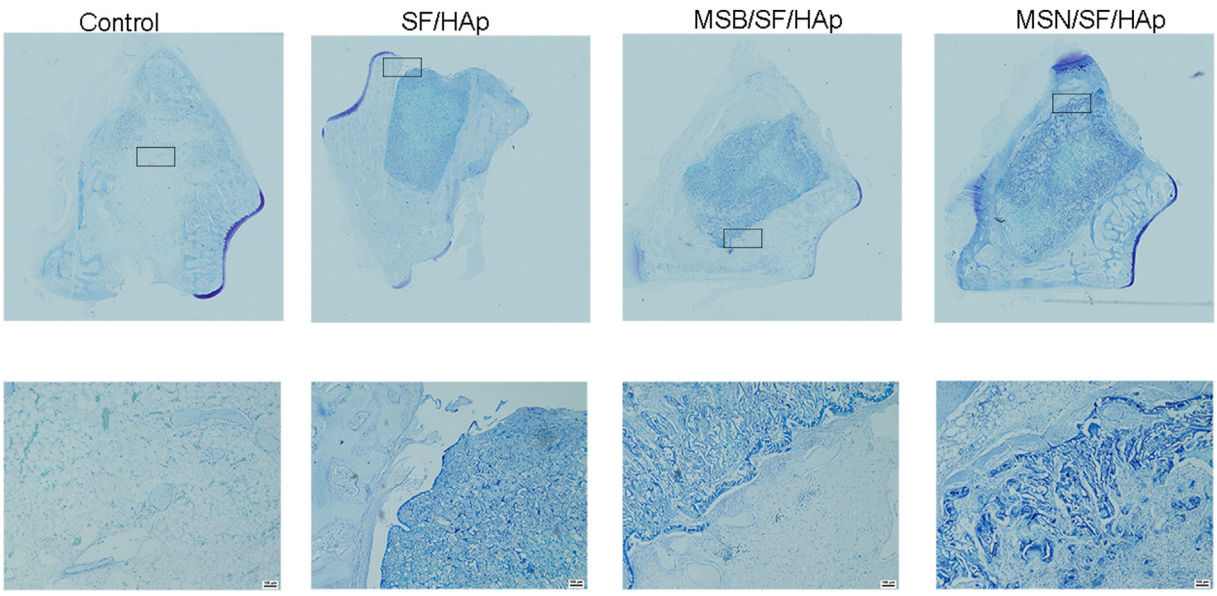

Fig. 11. Toluidine blue of defect area after implantation with different scaffolds for 6 weeks.

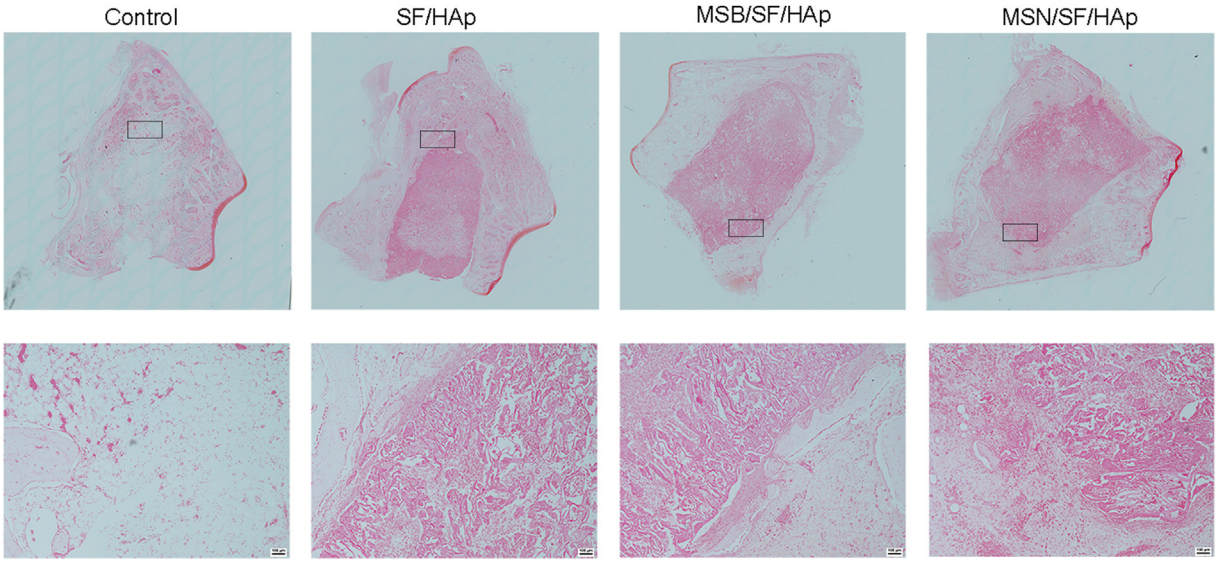

Fig. 12. Safranin-O staining of new bone areas in defect sites.

osteogenic differentiation assay and subsequently implanted in a rabbit femoral distal bone defect model. Our main findings showed that SF/HAp combined with naringin-loaded PLGA microspheres acted as effective naringin carriers, providing a diffusion-controlled naringin release profile. Thus, we generated naringin-encapsulated PLGA microspheres and sustained the release of naringin. Moreover, water-soluble SF was generated, and hexafluoroisopropanol was avoided as a solvent. We added cCNFs to improve the stability of HAp in an SF solution.

Naringin with PLGA microspheres showed sustained 30-day release of naringin from the microspheres. This study revealed that the encapsulation of naringin into PLGA microspheres prior to incorporation into an SF/HAp scaffold is an efficient strategy for delivering naringin in a prolonged and sustained release manner. Previously, simvastatin microspheres loaded into PLGA/HAp were developed as osteoinductive agents to treat severe bone defects [50]. Wang et al. [51] constructed an SF/HAp scaffold and found it suitable for bone regeneration. The microstructure of the SF/HAp scaffold was similar to that of natural human cancellous bone, and the average diameter of the SF/HAp scaffold was approximately 100 μm [52]. A pore diameter greater than 40 μm is required for osseous ingrowth; osteoid formation requires a minimum pore diameter of 100 μm [53].

Finally, we generated a novel SF/HAp scaffold with naringin release to promote the osteogenic differentiation of BMSCs and bone regeneration. In our study, ALP and ARS staining, qRT-PCR, and Western blot assays demonstrated that the SF/HAp scaffold with naringin microspheres could positively regulate the osteogenic differentiation of BMSCs and promote the differentiation of BMSCs into osteoblasts. Ge et al. [20] found that naringin exerted protective effects against glucocorticoid-induced osteoporosis via the PI3K/AKT/mTOR pathway. Our group found that naringin enhances fracture healing through the PI3K/Akt signaling pathway [22,23,54].

Moreover, we tested the mechanism of this novel scaffold for the osteogenic differentiation of BMSCs. We found that the MSN/SF/HAp scaffold positively regulated the Notch signaling pathway. Previously, we investigated the mechanism of naringin for osteogenic differentiation of human umbilical cord-derived mesenchymal stem cells in an SF/HAp

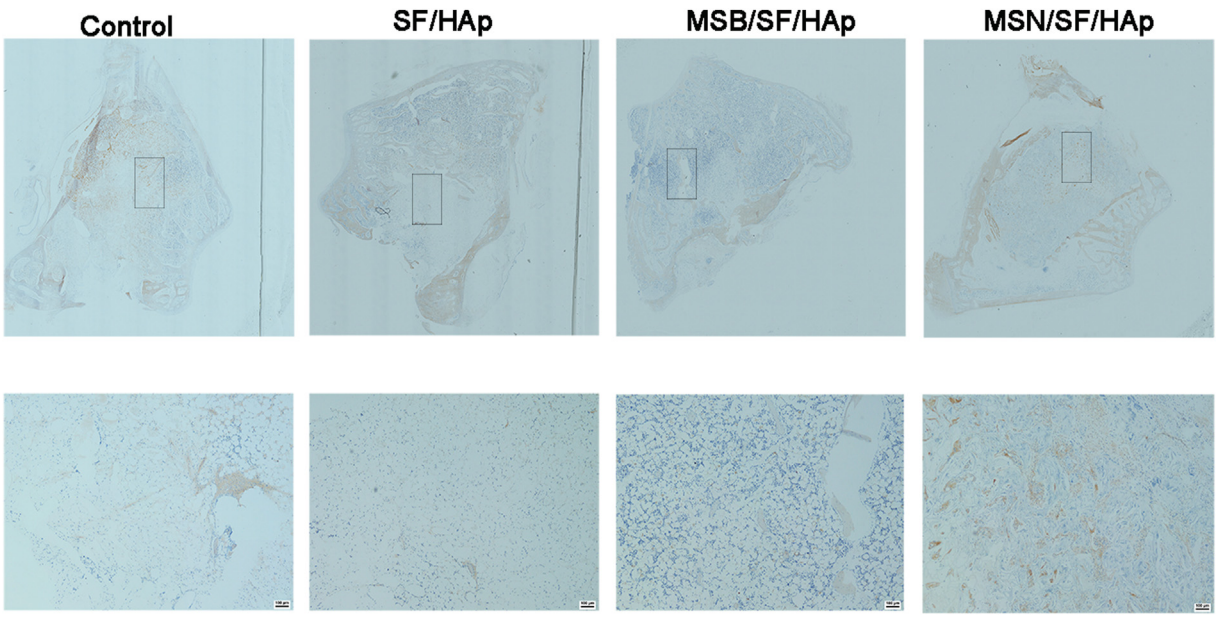

Fig. 13. Representative immunohistochemical staining of COL1A of the defected area after implantation with different scaffolds for 6 weeks.

scaffold inlaid with naringin [12]. The main enriched pathway was the PI3K/Akt signaling pathway. This suggests that the mechanism of MSN/SF/HAp is not the same as that of the naringin-inlaid SF/HAp scaffold.

Notch signaling critically regulates the fate of numerous cell types, including BMSCs and osteoblast [55–58]. Several studies have found that the Notch signaling pathway plays an important role in the osteogenic differentiation of BMSCs and the treatment of osteogenesis disorders [59–61]. Notch family members and their ligands balance the differentiation of osteoblasts [62]. Moreover, the Notch signaling pathway has been implicated as a regulator of vascular angiogenesis [63]. Moreover, notch signaling guides the initiation and stabilization of sprouting angiogenesis [64].

MSN/SF/HAp significantly increased bone formation in the rabbit femoral distal bone defect model after 6-week implantation. HAp is commonly used in clinical practice to promote bone regeneration because of its suitable bone induction properties [65]. The MSN/SF/HAp scaffold increased the expression levels of RUNX2, COL1A1, and OCN. The MSN/SF/HAp scaffold showed higher osteoinductivity in vivo, as evidenced by significantly higher BV/TV and TB. TH values. We performed HE, toluidine blue, and safranin O staining to assess bone regeneration of bone defects in the distal femur of rabbits. HE staining revealed that the MSN/SF/HAp scaffold markedly increased new bone formation in the defect area. Toluidine blue staining of more mineral tissue was observed more on the edge of the bone defect in MSN/SF/HAp than in the MSB/SF/HAp and SF/HAp groups. Moreover, MSN/SF/HAp significantly increased COL1A expression in the bone-defect area. COL1A provides a strong and flexible bone structure during osteoblast differentiation. A previous study conducted by Shao et al. [66] examined naringin in GelMA-incorporated rutile nanorod films, finding that these new films regulate the osteogenic differentiation of MSCs. Muhammad et al. [8] reviewed and pointed out that the SF/HAp scaffold is a highly compatible material for bone regeneration.

The present study had several limitations. First, no long-term observations of the rabbit distal femoral bone defect were performed. In addition, it involved a small animal model, and further investigation into whether the results of experimental animal studies can be generalized to humans is warranted.

5. Conclusion

Naringin-loaded PLGA microspheres were prepared and then incorporated into the SF/HAp scaffold to obtain the naringin-loaded composite scaffold (MSN/SF/HAp scaffold). In vitro assessments demonstrated that the MSN/SF/HAp scaffold exhibited a slow-release effect of naringin and supported the attachment, proliferation, and osteogenic differentiation of BMSCs. In vivo analysis indicated that MSN/SF/HAp promotes the repair of bone defects, thus providing a potential clinical candidate for BTE.

Consent for publication

All authors agree to be published.

Availability of data and materials

Complete data from this study can be obtained by contacting the corresponding author.

Authors' contributions

Zhihu Zhao: Data curation, writing of the original draft, investigation. Xinlong Ma: Investigation, review, and editing. Jianxiong Ma: Data curation/Jiayu Kang, Yue Guo, and Yang Zhang: Visualization and methodology. Xinlong Ma: Project administration and conceptualization.

Declaration of competing interest

The authors declare that they have no known competing financial interests or personal relationships that could have appeared to influence the work reported in this paper.

Acknowledgements

This study was supported by grants from the National Natural Science Foundation of China (Nos. 81871777, 81572154, 81501061, and 81401792), the Technology Fund of Tianjin Hospital (TJYY2117), and the Natural Science Foundation of Tianjin (ZC20068).

Appendix A. Supplementary data

Supplementary data to this article can be found online at https://doi.org/10.1016/j.mtbio.2022.100206.

References

[1] G. Buehrer, A. Balzer, I. Arnold, J.P. Beier, C. Koerner, O. Bleiziffer, et al., Combination of BMP2 and MSCs significantly increases bone formation in the rat arterio-venous loop model, Tissue Eng. 21 (2015) 96–105.

[2] Y. Leng, G. Ren, Y. Cui, C. Peng, J. Wang, D. Wu, et al., Platelet-rich plasma-enhanced osseointegration of decellularized bone matrix in critical-size radial defects in rabbits, Ann. Transl. Med. 8 (2020) 198.

[3] A.A. El-Rashidy, J.A. Roether, L. Harhaus, U. Kneser, A.R. Boccaccini, Regenerating bone with bioactive glass scaffolds: a review of in vivo studies in bone defect models, Acta Biomater. 62 (2017) 1–28.

[4] R. Fairag, L. Li, J.L. Ramirez-GarciaLuna, M.S. Taylor, B. Gaerke, M.H. Weber, et al., A composite lactide-mineral 3D-printed scaffold for bone repair and regeneration, Front. Cell Dev. Biol. 9 (2021) 654518.

[5] W. Li, K. Sheng, Y. Ran, J. Zhang, B. Li, Y. Zhu, et al., Transformation of acellular dermis matrix with dicalcium phosphate into 3D porous scaffold for bone regeneration, J. Biomater. Sci. Polym. Ed. (2021) 1–17.

[6] F. Mottaghitalab, H. Hosseinkhani, M.A. Shokrgozar, C. Mao, M. Yang, M. Farokhi, Silk as a potential candidate for bone tissue engineering, J. Contr. Release : official journal of the Controlled Release Society 215 (2015) 112–128.

[7] L. Meinel, R. Fajardo, S. Hofmann, R. Langer, J. Chen, B. Snyder, et al., Silk implants for the healing of critical size bone defects, Bone 37 (2005) 688–698.

[8] M. Saleem, S. Rasheed, C. Yougen, Silk fibroin/hydroxyapatite scaffold: a highly compatible material for bone regeneration, Sci. Technol. Adv. Mater. 21 (2020) 242–266.

[9] M. Farokhi, F. Mottaghitalab, S. Samani, M.A. Shokrgozar, S.C. Kundu, R.L. Reis, et al., Silk fibroin/hydroxyapatite composites for bone tissue engineering, Biotechnol. Adv. 36 (2018) 68–91.

[10] F. Coelho, M. Cavicchioli, S.S. Specian, E.M. Cilli, S.J. Lima Ribeiro, R.M. Scarel-Caminaga, et al., Silk fibroin/hydroxyapatite composite membranes: production, characterization and toxicity evaluation, Toxicol. Vitro : an international journal published in association with BIBRA 62 (2020) 104670.

[11] L. Wang, J.L. Pathak, D. Liang, N. Zhong, H. Guan, M. Wan, et al., Fabrication and characterization of strontium-hydroxyapatite/silk fibroin biocomposite nanospheres for bone-tissue engineering applications, Int. J. Biol. Macromol. 142 (2020) 366–375.

[12] Z.H. Zhao, X.L. Ma, B. Zhao, P. Tian, J.X. Ma, J.Y. Kang, et al., Naringin-inlaid silk fibroin/hydroxyapatite scaffold enhances human umbilical cord-derived mesenchymal stem cell-based bone regeneration, Cell Prolif 54 (2021), e13043.

[13] H. Wang, C. Li, J. Li, Y. Zhu, Y. Jia, Y. Zhang, et al., Naringin enhances osteogenic differentiation through the activation of ERK signaling in human bone marrow mesenchymal stem cells, Iranian journal of basic medical sciences 20 (2017) 408–414.

[14] G.Y. Yu, G.Z. Zheng, B. Chang, Q.X. Hu, F.X. Lin, D.Z. Liu, et al., Naringin stimulates osteogenic differentiation of rat bone marrow stromal cells via activation of the notch signaling pathway, Stem Cell. Int. 2016 (2016) 7130653.

[15] E.S. Ang, X. Yang, H. Chen, Q. Liu, M.H. Zheng, J. Xu, Naringin abrogates osteoclastogenesis and bone resorption via the inhibition of RANKL-induced NF-κB and ERK activation, FEBS Lett. 585 (2011) 2755–2762.

[16] F. Li, X. Sun, J. Ma, X. Ma, B. Zhao, Y. Zhang, et al., Naringin prevents ovariectomy-induced osteoporosis and promotes osteoclasts apoptosis through the mitochondria-mediated apoptosis pathway, Biochem. Biophys. Res. Commun. 452 (2014) 629–635.

[17] J. An, H. Yang, Q. Zhang, C. Liu, J. Zhao, L. Zhang, et al., Natural products for treatment of osteoporosis: the effects and mechanisms on promoting osteoblast-mediated bone formation, Life Sci. 147 (2016) 46–58.

[18] W. Wang, J. Mao, Y. Chen, J. Zuo, L. Chen, Y. Li, et al., Naringin promotes osteogenesis and ameliorates osteoporosis development by targeting JAK2/STAT3 signalling, Clin. Exp. Pharmacol. Physiol. 49 (2022) 113–121.

[19] N. Li, Y. Jiang, P.H. Wooley, Z. Xu, S.Y. Yang, Naringin promotes osteoblast differentiation and effectively reverses ovariectomy-associated osteoporosis, J. Orthop. Sci. : official journal of the Japanese Orthopaedic Association 18 (2013) 478–485.

[20] X. Ge, G. Zhou, Protective effects of naringin on glucocorticoid-induced osteoporosis through regulating the PI3K/Akt/mTOR signaling pathway, Am. J. Tourism Res. 13 (2021) 6330–6341.

[21] A.D. Kandhare, P. Ghosh, S.L. Bodhankar, Naringin, a flavanone glycoside, promotes angiogenesis and inhibits endothelial apoptosis through modulation of inflammatory and growth factor expression in diabetic foot ulcer in rats, Chem. Biol. Interact. 219 (2014) 101–112.

[22] N. Song, Z. Zhao, X. Ma, X. Sun, J. Ma, F. Li, et al., Naringin promotes fracture healing through stimulation of angiogenesis by regulating the VEGF/VEGFR-2 signaling pathway in osteoporotic rats, Chem. Biol. Interact. 261 (2017) 11–17.

[23] Z. Zhao, X. Ma, J. Ma, X. Sun, F. Li, J. Lv, Naringin enhances endothelial progenitor cell (EPC) proliferation and tube formation capacity through the CXCL12/CXCR4/PI3K/Akt signaling pathway, Chem. Biol. Interact. 286 (2018) 45–51.

[24] Y.T. Fong, C.H. Chen, J.P. Chen, Intratumoral delivery of doxorubicin on folate-conjugated graphene oxide by in-situ forming thermo-sensitive hydrogel for breast cancer therapy, Nanomaterials 7 (2017) 388.

[25] S. Siddique, J. Khanam, P. Bigoniya, Development of sustained release capsules containing "coated matrix granules of metoprolol tartrate, AAPS PharmSciTech 11 (2010) 1306–1314.

[26] E.E. El Naggar, E.A. Mohamed, Colon targeting of naringin for enhanced cytoprotection against indomethacin-induced colitis in rabbits, Drug Des. Dev. Ther. 14 (2020) 677–696.

[27] S. Mohanty, V.B. Konkimalla, A. Pal, T. Sharma, S.C. Si, Naringin as sustained delivery nanoparticles ameliorates the anti-inflammatory activity in a freund's complete adjuvant-induced arthritis model, ACS Omega 6 (2021) 28630–28641.

[28] X. Wang, X. Wu, H. Xing, G. Zhang, Q.E.L. Shi, et al., Porous nanohydroxyapatite/collagen scaffolds loading insulin PLGA particles for restoration of critical size bone defect, ACS Appl. Mater. Interfaces 9 (2017) 11380–11391.

[29] F. Nan, J. Wu, F. Qi, Q. Fan, G. Ma, T. Ngai, Preparation of uniform-sized colloidosomes based on chitosan-coated alginate particles and its application for oral insulin delivery, J. Mater. Chem. B 2 (2014) 7403–7409.

[30] F. Barry, R.E. Boynton, B. Liu, J.M. Murphy, Chondrogenic differentiation of mesenchymal stem cells from bone marrow: differentiation-dependent gene expression of matrix components, Exp. Cell Res. 268 (2001) 189–200.

[31] K. Ishii, T. Furuta, Y. Kasuya, Determination of naringin and naringenin in human urine by high-performance liquid chromatography utilizing solid-phase extraction, J. Chromatogr. B Biomed. Sci. Appl. 704 (1997) 299–305.

[32] S. Changotade, G. Radu Bostan, A. Consalus, F. Poirier, J. Peltzer, J.J. Lataillade, et al., Preliminary in vitro assessment of stem cell compatibility with cross-linked poly(ε-caprolactone urethane) scaffolds designed through high internal phase emulsions, Stem Cell. Int. 2015 (2015) 283796.

[33] M. Dominici, K. Le Blanc, I. Mueller, I. Slaper-Cortenbach, F. Marini, D. Krause, et al., Minimal criteria for defining multipotent mesenchymal stromal cells. The International Society for Cellular Therapy position statement, Cytotherapy 8 (2006) 315–317.

[34] S. Watanabe, H. Fujii, K. Kono, K. Watanabe, S. Goto, S. Nishi, Influence of oxidative stress on vascular calcification in the setting of coexisting chronic kidney disease and diabetes mellitus, Sci. Rep. 10 (2020) 20708.

[35] C.A. Gregory, W.G. Gunn, A. Peister, D.J. Prockop, An Alizarin red-based assay of mineralization by adherent cells in culture: comparison with cetylpyridinium chloride extraction, Anal. Biochem. 329 (2004) 77–84.

[36] C. Kilkenny, W.J. Browne, I.C. Cuthill, M. Emerson, D.G. Altman, Improving bioscience research reporting: the ARRIVE guidelines for reporting animal research, J. Pharmacol. Pharmacother. 1 (2010) 94–99.

[37] X. Yi, W. Zeng, C. Wang, Y. Chen, L. Zheng, X. Zhu, et al., A step-by-step multiple stimuli-responsive metal-phenolic network prodrug nanoparticles for chemotherapy, Nano Res. (2021) 1–8.

[38] Y. Kuang, J. Zhang, M. Xiong, W. Zeng, X. Lin, X. Yi, et al., A novel nanosystem realizing curcumin delivery based on Fe3O4@ carbon dots nanocomposite for Alzheimer's disease therapy, Front. Bioeng. Biotechnol. 8 (2020).

[39] X. Sun, X. Li, H. Qi, X. Hou, J. Zhao, X. Yuan, et al., MiR-21 nanocapsules promote early bone repair of osteoporotic fractures by stimulating the osteogenic differentiation of bone marrow mesenchymal stem cells, Journal of orthopaedic translation 24 (2020) 76–87.

[40] Y. Shi, R. He, X. Deng, Z. Shao, D. Deganello, C. Yan, et al., Three-dimensional biofabrication of an aragonite-enriched self-hardening bone graft substitute and assessment of its osteogenicity in vitro and in vivo, Biomaterials Translational 1 (2020) 69–81.

[41] C. Xie, J. Ye, R. Liang, X. Yao, X. Wu, Y. Koh, et al., Advanced strategies of biomimetic tissue-engineered grafts for bone regeneration, Advanced healthcare materials 10 (2021) e2100408.

[42] J. Ng, K. Spiller, J. Bernhard, G. Vunjak-Novakovic, Biomimetic approaches for bone tissue engineering. Tissue engineering Part B, Review 23 (2017) 480–493.

[43] L. Zhang, X. Li, C. Shi, Biocompatibility and angiogenic effect of chitosan/graphene oxide hydrogel scaffolds on EPCs, Stem Cell. Int. 2021 (2021) 5594370.

[44] N. Ashari, H.W. Pang, T. Simon, Y. Xiong, J.M. Coburn, J.S. Bromberg, et al., Silk fibroin preserves beta cell function under inflammatory stress while stimulating islet cell surface GLUT2 expression, Cell. Immunol. 329 (2018) 10–16.

[45] M.S.B. Reddy, D. Ponnamma, A comparative review of natural and synthetic biopolymer composite scaffolds, Polymers 13 (2021) 1105.

[46] J. Wu, K. Zheng, X. Huang, J. Liu, H. Liu, A.R. Boccaccini, et al., Thermally triggered injectable chitosan/silk fibroin/bioactive glass nanoparticle hydrogels for in-situ bone formation in rat calvarial bone defects, Acta Biomater. 91 (2019) 60–71.

[47] S. Mondal, P. Manivasagan, S. Bharathiraja, M. Santha Moorthy, V.T. Nguyen, H.H. Kim, et al., Hydroxyapatite coated iron oxide nanoparticles: a promising nanomaterial for magnetic hyperthermia cancer treatment, Nanomaterials 7 (2017).

[48] F.A. Sheikh, H.W. Ju, B.M. Moon, H.J. Park, J.H. Kim, O.J. Lee, et al., A novel approach to fabricate silk nanofibers containing hydroxyapatite nanoparticles using a three-way stopcock connector, Nanoscale Res. Lett. 8 (2013) 303.

[49] S. Li, B.D. Vogt, Aqueous polypropylene glycol induces swelling and severe plasticization of high T(g) amphiphilic copolymers containing hexafluoroisopropanol groups, Soft Matter 16 (2020) 6362–6370.

[50] I.C. Tai, Y.C. Fu, C.K. Wang, J.K. Chang, M.L. Ho, Local delivery of controlled-release simvastatin/PLGA/HAp microspheres enhances bone repair, Int. J. Nanomed. 8 (2013) 3895–3904.

[51] Q. Wang, Y. Zhang, B. Li, L. Chen, Controlled dual delivery of low doses of BMP-2 and VEGF in a silk fibroin-nanohydroxyapatite scaffold for vascularized bone regeneration, J. Mater. Chem. B 5 (2017) 6963–6972.

[52] J.E. Song, N. Tripathy, Quercetin inlaid silk fibroin/hydroxyapatite scaffold promotes enhanced osteogenesis, ACS Appl. Mater. Interfaces 10 (2018) 32955–32964.

[53] D.N. Bracey, T.M. Seyler, A decellularized porcine xenograft-derived bone scaffold for clinical use as a bone graft substitute: a critical evaluation of processing and structure, J. Funct. Biomater. 9 (2018).
[54] X. Sun, F. Li, X. Ma, J. Ma, B. Zhao, Y. Zhang, et al., The effects of combined treatment with naringin and treadmill exercise on osteoporosis in ovariectomized rats, Sci. Rep. 5 (2015) 13009.
[55] C. Wang, J.A. Inzana, A.J. Mirando, Y. Ren, Z. Liu, J. Shen, et al., NOTCH signaling in skeletal progenitors is critical for fracture repair, J. Clin. Invest. 126 (2016) 1471–1481.
[56] Q. Xing, Q. Ye, M. Fan, Y. Zhou, Q. Xu, A. Sandham, Porphyromonas gingivalis lipopolysaccharide inhibits the osteoblastic differentiation of preosteoblasts by activating Notch1 signaling, J. Cell. Physiol. 225 (2010) 106–114.
[57] S. Zanotti, E. Canalis, Notch signaling and the skeleton, Endocr. Rev. 37 (2016) 223–253.
[58] S.K. Ramasamy, A.P. Kusumbe, L. Wang, R.H. Adams, Endothelial Notch activity promotes angiogenesis and osteogenesis in bone, Nature 507 (2014) 376–380.
[59] K. Sottoriva, K.V. Pajcini, Notch signaling in the bone marrow lymphopoietic niche, Front. Immunol. 12 (2021) 723055.
[60] A. Guasto, V. Cormier-Daire, Signaling pathways in bone development and their related skeletal dysplasia, Int. J. Mol. Sci. 22 (2021).
[61] M. Pakvasa, P. Haravu, M. Boachie-Mensah, A. Jones, E. Coalson, J. Liao, et al., Notch signaling: its essential roles in bone and craniofacial development, Genes & diseases 8 (2021) 8–24.
[62] K. Tezuka, M. Yasuda, N. Watanabe, N. Morimura, K. Kuroda, S. Miyatani, et al., Stimulation of osteoblastic cell differentiation by Notch, J. Bone Miner. Res. : the official journal of the American Society for Bone and Mineral Research 17 (2002) 231–239.
[63] Y. Peng, S. Wu, Y. Li, J.L. Crane, Type H blood vessels in bone modeling and remodeling, Theranostics 10 (2020) 426–436.
[64] A. Al Haj Zen, P. Madeddu, Notch signalling in ischaemia-induced angiogenesis, Biochem. Soc. Trans. 37 (2009) 1221–1227.
[65] Y. Qin, J. Guan, C. Zhang, Mesenchymal stem cells: mechanisms and role in bone regeneration, Postgrad. Med. 90 (2014) 643–647.
[66] Y. Shao, D. You, Y. Lou, J. Li, B. Ying, K. Cheng, et al., Controlled release of naringin in GelMA-incorporated rutile nanorod films to regulate osteogenic differentiation of mesenchymal stem cells, ACS Omega 4 (2019) 19350–19357.